Int J Earth Sci (Geol Rundsch) (2017) 106:1161–1174
DOI 10.1007/s00531-016-1350-z

ORIGINAL PAPER

Orbital-driven environmental changes recorded at ODP Site 959 (eastern equatorial Atlantic) from the Late Miocene to the Early Pleistocene

Francesca Vallé[1] · Thomas Westerhold[1] · Lydie M. Dupont[1]

Received: 10 February 2016 / Accepted: 31 May 2016 / Published online: 14 June 2016

Abstract Palaeorecords from tropical environments are important to explore the linkages between precipitation, atmospheric circulation and orbital forcing. In this study, new high-resolution XRF data from ODP Site 959 (3°37′N, 2°44′W) have been used to investigate the relationship between palaeoenvironmental changes in West Africa and sedimentation in the tropical East Atlantic Ocean. Iron intensity data have been used to build a 91-m composite depth record that has been astronomically tuned allowing the development of a detailed age model from 6.2 to 1.8 Ma. Based on this new stratigraphy, we studied the variations of Ti/Al, Ti/Ca and Al/Si ratios, proxies for aeolian versus fluvial supply, as dust indicator and fine versus coarse grain size, respectively. We discuss sedimentation patterns at ODP Site 959 associated with the environmental changes from the late Miocene until the early Pleistocene. During the interval corresponding to the earlier stages of the Messinian Salinity Crisis, our proxy records indicate enhanced run-off from the West African continent and major supply of fine material at ODP Site 959, suggesting a stronger monsoon and increased precipitation during eccentricity minima. A long-term decrease of river supply is documented after 5.4 Ma until the end of the Pliocene. From the increased values and variability of Ti/Al and Ti/Ca ratios, we suggest that after 3.5 Ma dust started to reach the study site probably as a result of the southward shift of the Intertropical Convergence Zone during winter. Between 3.2 and 2.9 Ma, ODP Site 959 Ti/Ca ratios exhibit three maxima corresponding to eccentricity maxima similarly to other dust records of northern Africa. This suggests continent-wide aridity or larger climate variability during that interval. Eccentricity forcing (405 and 100 kyr) and precession frequencies are found in the entire studied interval. The variations of Ti/Al ratio suggest stronger seasonality between 5.8 and 5.5 Ma and after 3.2 Ma.

Keywords Pliocene · XRF core scanning · Astronomical tuning · West Africa · Ivory Basin · Terrestrial input

Introduction

Pliocene climate, especially the mid-Piacenzian warm period, has been used as an analogue to understand warmer climates (review of Haywood et al. 2016 and references therein), and Africa is one of the more vulnerable continents to climate change and climate variability (Boko et al. 2007). The climate of northern Africa reaches from the Mediterranean to the equatorial tropics and forms a link between low and high latitudes. Northern African climate is driven by changes in sea surface temperatures and wind systems being dominated by the African Monsoon (Norris 1998), which is subject to the latitudinal migration of the Intertropical Convergence Zone (ITCZ) (Ruddiman et al. 1989) and the African rainbelt (Nicholson 2009). It is tied to the Mediterranean Sea via the impact of the African monsoon and resulting river discharge on the deep water circulation of the Mediterranean Sea (Rossignol-Strick et al. 1982; Rohling et al. 2015). On the other hand, the Messinian Salinity Crisis at the end of the Miocene

Electronic supplementary material The online version of this article (doi:10.1007/s00531-016-1350-z) contains supplementary material, which is available to authorized users.

✉ Lydie M. Dupont
ldupont@marum.de

[1] MARUM-Center for Marine Environmental Sciences, Leobener Strasse, 28359 Bremen, Germany

potentially affected the climate of northern Africa (Murphy et al. 2009; Schneck et al. 2010).

Although the late Miocene to Pliocene northern African climate was warmer and wetter than in the Pleistocene and today, fluctuations between arid and wet periods occurred since at least 8 Ma (Larrasoaña et al. 2013). During these cycles, interactions between vegetation cover, rainfall and dust formation are mainly controlled by the African summer monsoon oscillating in synch with Earth's orbital precession cycles (deMenocal 2011; Zhang et al. 2014). The impact of eccentricity on tropical climate is thought to be via the modulation of the precession, which controls the distribution of insolation between hemispheres and has strong influence on the monsoon (e.g. Kutzbach and Liu 1997). Modelling studies have shown that both precession and obliquity intensify precipitation in northern Africa but that precession only influences the seasonal timing of the occurrence of the precipitation maximum (Tuenter et al. 2003).

During more arid periods, dust supply from the African continent to the East Atlantic Ocean was enhanced while it was reduced during more wet intervals. Dust flux records at different locations offshore of West Africa indicate aeolian supply from the African continent to the East Atlantic Ocean since at least 8 Ma (Ruddiman et al. 1989). Recent modelling studies even suggest a much earlier expansion of the Sahara Desert linked to the closure of the Tethys basins dating back to the Tortonian Stage (11.6–7.2 Ma) (Zhang et al. 2014), well before the Messinian Salinity Crisis (MSC; 5.96–5.33 Ma) in which the Mediterranean Basin was partly isolated from the Atlantic Ocean (Krijgsman et al. 1999).

The Mediterranean deep water formation had been weakened since 7.2 Ma (Kouwenhoven and Van der Zwaan 2006). However, the connection between the Mediterranean Sea and the Atlantic Ocean remained open until 5.61 Ma (Topper and Meijer 2013). This connection was severed between 5.61 and 5.55 Ma and the Mediterranean basin desiccated almost completely. Desiccation had already begun shortly before 6.2 Ma creating salty and dense waters flowing into the Atlantic and contributed to North Atlantic Deep Water formation until 6.0 Ma (Pérez-Asensio et al. 2012). The last stage of the MCS lasted from 5.55 to 5.33 Ma in which the Mediterranean Sea was still mostly isolated from the Atlantic Ocean until the connection re-established rather abruptly after 5.33 Ma (CIESM 2008; Roveri et al. 2014). Fluctuations in the amount and salinity of the Mediterranean Outflow Water between 6.0 and 5.5 Ma could have influenced the strength and position of the Atlantic Overturning Circulation. Modelling shows that this would have affected the meridional heat distribution, although the effects on climate outside the North Atlantic region are small (Ivanovic et al. 2014). Model sensitivity experiments indicate changes in the rainfall pattern of northern Africa as the result of the desiccation and/or lower sea levels in the Mediterranean Basin (Murphy et al. 2009; Schneck et al. 2010).

An important issue about Pliocene climate is the increasing zonal and meridional temperature gradients leading to intensified Walker and Hadley circulations (Wara et al. 2005; Brierley et al. 2009; Brierley and Fedorov 2010; Fedorov et al. 2013). At the end of the Pliocene, a major increase of dust supply from the Sahel and Sahara into the East Atlantic Ocean at 2.7 Ma is the result of intensified aridity in northern Africa (Tiedemann et al. 1994; deMenocal 1995). The aridity is probably caused by enhanced NE Trade winds in relation to the northern hemisphere glaciations associated with decreased sea surface temperatures (SST) of the North Atlantic (Lawrence et al. 2010) and increased seasonality (Hennissen et al. 2015). At the same time, dust records from the southern ocean (Martínez-Garcia et al. 2011) and the North Atlantic also show increase in dust accumulation (Naafs et al. 2012). The latter has been related to increased dust production in North America after the intensification of the northern hemisphere glaciations (Naafs et al. 2012; Bailey et al. 2013; Lang et al. 2014).

Indications about the response of precipitation and atmospheric circulation to past climate changes have been derived from tropical palaeoenvironmental records (McGee et al. 2014). Whereas many records concerning subtropical northern Africa exist, the magnitude and regional variability of the African monsoon in the past are poorly constrained (McGee et al. 2014). To obtain new insights into the environmental evolution linked to latitudinal shifts of the rainbelt and the ITCZ in near-equatorial West Africa during the Late Miocene to Early Pleistocene, we investigated the fluctuations in proxy records of siliciclastic supply at Ocean Drilling Program (ODP) Site 959 retrieved offshore of Ivory Coast. We present new high-resolution data obtained by X-ray fluorescence (XRF) scanning of marine sediment cores. We used the iron (Fe) record to develop a detailed age model by orbital tuning. Based on this age model, we analysed the sedimentation patterns at ODP Site 959. We discuss our results together with the magnetic susceptibility record of the same site, available at the ODP Janus database, and compare them with proxy records from other sites from the equatorial East Atlantic (ODP Site 662), the tropical East Atlantic (ODP Site 659) and the Arabian Sea (ODP Site 721/722).

Study site, materials and methods

ODP Site 959 was drilled in 1995 during Leg 159 on a small plateau on the southern shoulder of the Deep Ivorian Basin at 3°37′N, 2°44′W and 2100 m water depth, ~120 km offshore of Ivory Coast (Fig. 1). The modern oceanographic setting of

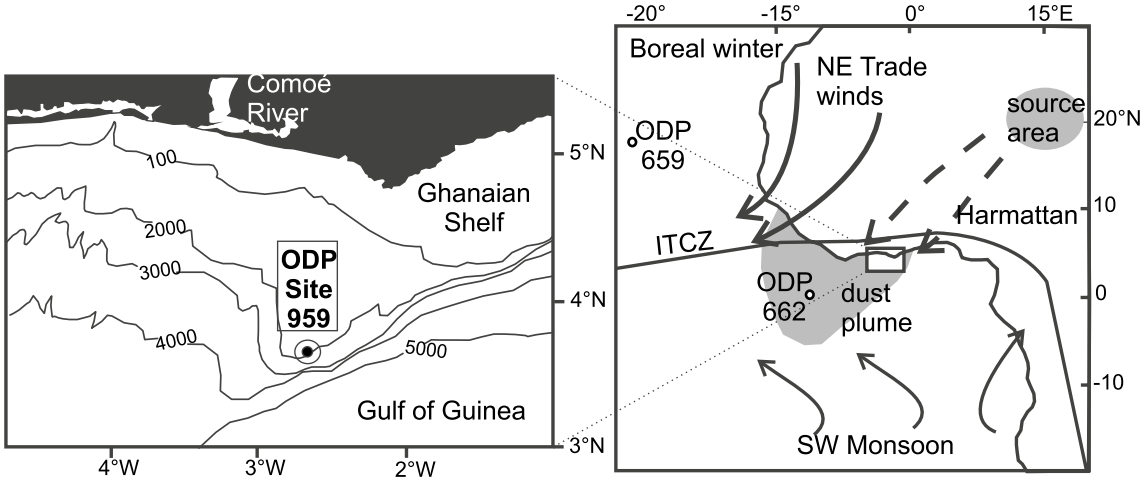

Fig. 1 *Left* Location of ODP Site 959 in the Ivory Basin. *Right* Atmospheric circulation and aeolian transport over West Africa during boreal winter. *Solid thick arrows* represent NE Trade Winds; *solid thin arrows* represent SW Monsoon. *Dashed arrows* indicate the direction of the Harmattan. *Grey areas* denote the dust source area and the corresponding dust plume reaching ODP Site 959 following Kalu (1979). Redrawn from Norris (1998) and Wagner (1998). Localities of ODP site 659 and ODP site 662 used for comparison are shown with *open circles*

ODP Site 959 is characterized by coastal upwelling in boreal summer as the result of the Guinea Current combined with winds flowing parallel along the coast (Verstraete 1992).

The siliciclastic component deposited at ODP Site 959 is mainly aeolian (Wagner 1998). During boreal winter, when the ITCZ is at its southern position, the flows of the Harmattan (Kalu 1979) and the enhanced NE Trade winds reach the Gulf of Guinea carrying dust particles mostly from the north-eastern part of the Sahara desert and the Sahel zone (Kalu 1979; Sarnthein et al. 1981; Prospero et al. 2002) (Fig. 1). Today, river discharge along the coastline is moderate and most of the mass gravitational flows are canalized into the Deep Ivorian Basin (Giresse et al. 1998). Fluvial material thus does not often reach Site 959 (Wagner 1998). The Late Miocene-Early Pleistocene sections of ODP Site 959 constitute of bioturbated nannofossil-foraminifera oozes with clay and chalk starting from ~75 m below sea floor (Mascle et al. 1996).

The published stratigraphic framework for ODP Site 959 from the Cretaceous to the Quaternary is based on shipboard biostratigraphy (Wagner 2002). Magnetostratigraphy could not be established at Site 959 because of the low magnetic properties of the sediments (Mascle et al. 1996). No previous attempts have been made to generate a splice record for our target interval. We use XRF core scanning data generated on Holes A, B and C to check whether cores can be spliced together to form a composite record. At tie-points between cores we routinely have XRF data of two holes overlapping each other sufficiently (50–100 cm) to secure the tie-point. We constructed a splice for cores 3H-9H from Hole 159-959A, cores 3H-11H from Hole 159-959B and cores 4H-11H from Hole 159-959C.

We used the XRF Core Scanner II at the MARUM-University of Bremen which enables almost a continuous and non-destructive analysis of major elements (Röhl and Abrams 2000; Röhl et al. 2007; Westerhold et al. 2007). To prevent contamination and desiccation of the sediment, the split surface of the sections were covered with a 4 µm thin Ultralene foil. Disturbed parts of the sections were not scanned, whereas overlapping sections for at least two holes were scanned in order to obtain a complete record. The measurements of the major light elements were collected every 1 cm down-core over 1 cm^2 using a generator setting of 10 kV and 20 s counting time. The scanning data had a high signal-to-noise ratio.

We used iron (Fe) intensity data (area—number of total counts in 20 s) to correlate between holes, construct a splice record (supplementary information) and develop the age model. From the intensities of titanium (Ti), calcium (Ca), aluminium (Al) and silicon (Si), we calculated Ti/Ca, Ti/Al and Al/Si ratios to use as environmental indicators (discussed in section "Interpretation of the elemental ratios in the sediment"). We prefer ratios over intensity data because the intensities are effectively proportions that suffer from dilution effects. To counter the asymmetry inherent to ratios, we applied a natural log transformation ensuring the symmetry of those ratios around zero (Weltje and Tjallingii 2008; Govin et al. 2012).

Results

The intensities of Fe, Ti, Al, Si and Ca show similar cyclic oscillations in each of the measured holes (Fig. 2). Fe, Si,

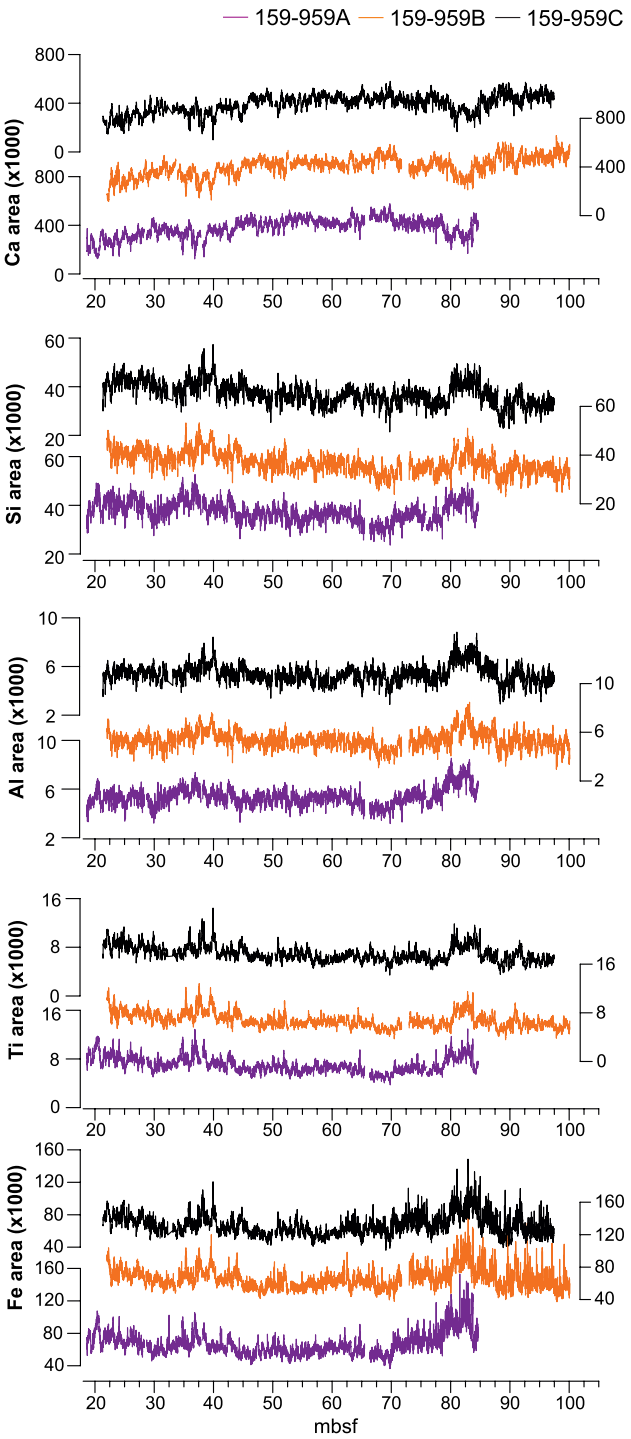

Fig. 2 Element areas (intensities) against metre below sea floor (mbsf) measured with XRF scanning at 1-cm resolution for ODP Leg 159-959A (*violet*) Cores 3–9, 159-959B Cores 4–11 (*orange*) and 159-959C cores 4–11 (*black*)

Al, Ti intensities show opposite patterns to those of Ca reflecting the different origins of those elements. The measured elemental intensities are related to the concentration

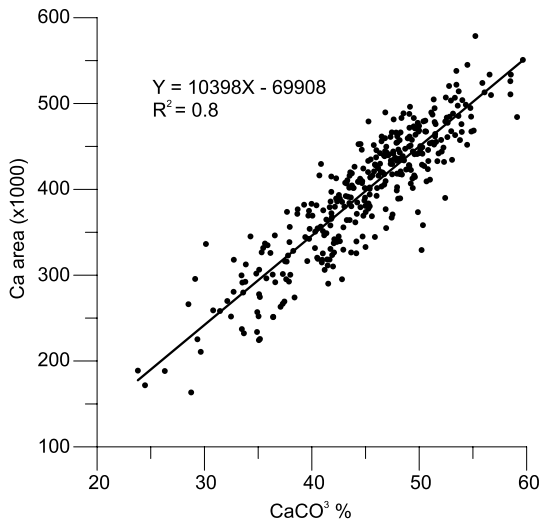

Fig. 3 Correlation between XRF scanning measurements of calcium intensities and carbonate content measured on discrete samples (Wagner 2002)

of the elements in the sediments. In our records, Ca and Fe intensities are one order of magnitude higher than those of Si, Al and Ti. Comparison between calcium intensities and carbonate content data measured on discrete samples (Wagner 2002) shows a linear correlation establishing that variations of Ca intensities between 250,000 and 450,000 counts per area reflect a carbonate content varying between 31 and 50 %, respectively (Fig. 3). The amplitude of the intensity fluctuations is higher between 45 and 34 mbsf and between 85 and 80 mbsf. Those intervals indicate a relative decrease in calcium and increase in terrigenous elements. Fe intensities show clear prominent features that we subsequently used to construct the composite depth scale. All scanning data are stored at Pangaea.de http://doi.pangaea.de/10.1594/PANGAEA.858040.

Development of the age model

High-resolution XRF core scanning data measured on multiple holes (Supplementary Fig. 1) were used to build a composite depth scale for the site (e.g. Evans et al. 2004; Westerhold et al. 2005, 2012; Westerhold and Röhl 2013), which required several steps (supplementary information, Supplementary Tables 1–3). The cyclic patterns in the depth domain were then orbitally tuned in order to develop a high-resolution age model.

After detrending the data, we proceeded with time series analysis in depth and frequency domains to establish whether the rhythms shown in the Fe composite record are related to Milankovitch cycles (supplementary

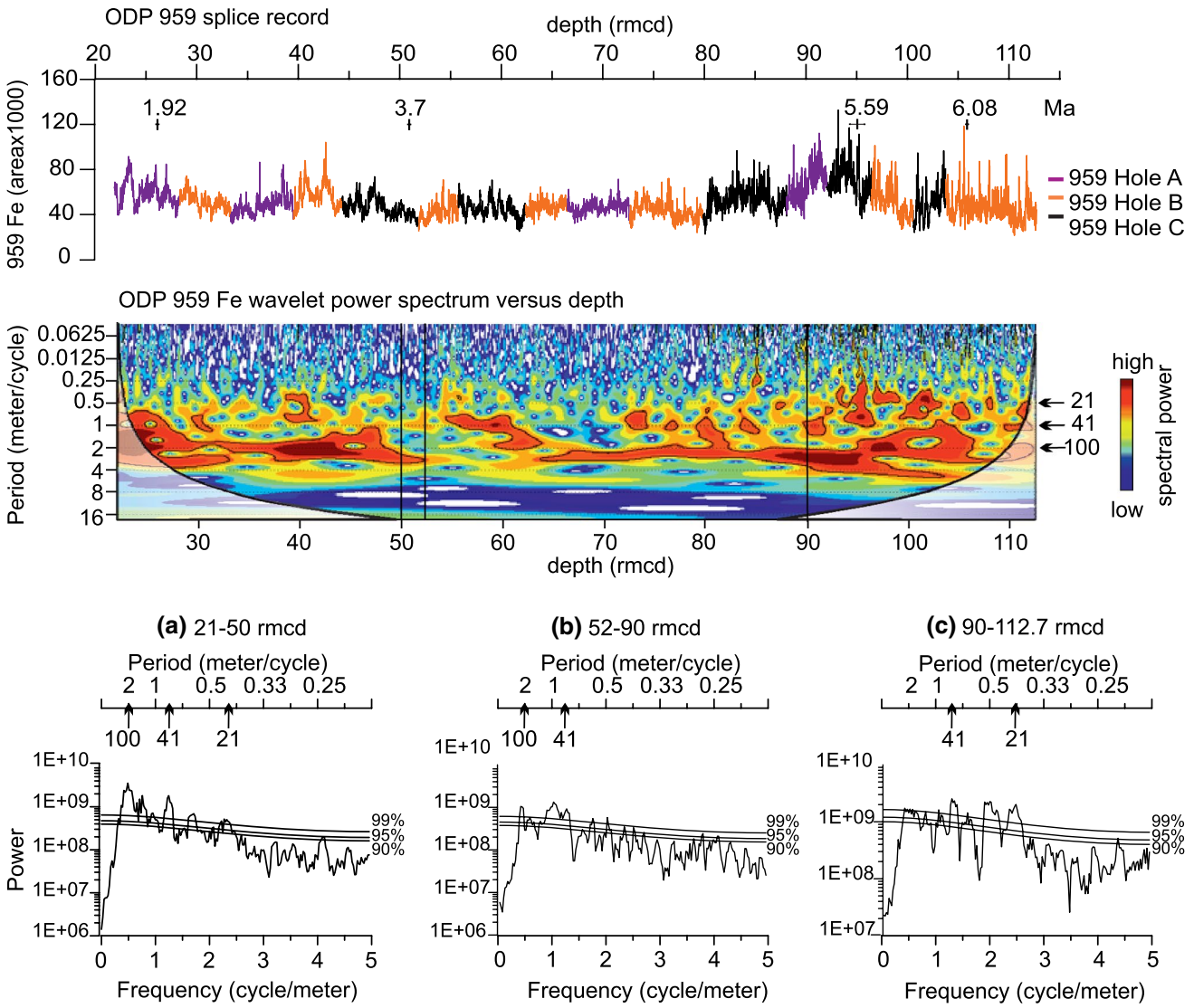

Fig. 4 *Top* ODP Site 959 splice record on revised composite depth in metre (rmcd). *Middle* Wavelet (Morlet) power spectrum of Fe intensity in the depth domain from 21.9 to 112.7 m composite depth (rmcd). The *contours* are normalized linear variances with *blue* representing low spectral power and *red* representing high spectral power. The *black contour lines* enclose regions with more than 95 % confidence based on white noise. *Shaded areas* on either end indicate the cone of influence where padding with zeros influences the results. *Bottom* (**a**–**c**) MTM power spectra of Fe intensity data in the depth domain for three intervals. Calculated confidence levels (90 %, 95 %, 99 %) based on a robust *red* noise estimation (Mann and Lees 1996) are shown. Wavelet analysis was calculated with software provided by Torrence and Compo. Multitaper Method (MTM) spectra were calculated by the kSpectra Toolkit software from SpectraWorks using three tapers and a resolution of 2. Prior to time series analysis, Fe data were detrended and linearly resampled at 1 cm and outliers were removed

information). As suggested by Weedon (2003), the usage of evolutionary spectra in the depth domain allows the identification of dominant cycle periods and changes of those periods over the entire record. We chose the wavelet analysis (Morlet wavelet) to calculate evolutionary spectra (Torrence and Compo 1998). Wavelet software was provided by C. Torrence and G. Compo (atoc.colorado.edu/research/wavelets/). Multitaper Method (MTM) power spectra (Fig. 4) were calculated by the kSpectra Toolkit software from SpectraWorks using three tapers and a resolution of 2 (Ghil et al. 2002). Confidence levels are based on a robust red noise estimation (Mann and Lees 1996). Evolutionary wavelet spectra of the ODP Site 959 Fe intensity record evidence high spectral power in parallel bands at three distinct periods (Fig. 4). The dominant cycle throughout the record is 2 m long. Only between 52 and 62 rmcd, this

cycle becomes less evident in the wavelet spectra. Shorter cycles (1, 0.5 and 0.4 m, respectively) are expressed from 52 rmcd until the base of the record.

The absence of strong shifts of the period bands in the wavelet spectra indicate that rapid changes of sedimentation rate did not occur in the studied interval. We assume relatively constant sedimentation rates within three intervals; 21–50 rmcd (Fig. 4a), 52–90 rmcd (Fig. 4b), and 90–112.7 rmcd (Fig. 4c). Multitaper spectra have been calculated for those intervals. The frequencies obtained are in accordance with the periodicities of the wavelet analysis. Frequencies around 0.5 cycle/m (2 m/cycle) of the upper interval have higher power than those of the lower interval. High power around the 2-cycle/m-frequency (0.5 m/cycle) within the interval between 90 and 112.7 rmcd is linked with the high variability in the Fe intensity data. Applying the biostratigraphic ages (Supplementary Table 4) and the resulting sedimentation rates, we estimated that the 2-m-cycle represents the mean short eccentricity cycle (100 kyr), the 1-m-cycle the obliquity component (41 kyr), and the 0.5–0.4-m-cycles the mean precession component (21 kyr). Spectral analysis of the lower part of the record (Fig. 4c) reveals a split peak (calculated frequencies of 2 and 2.4 cycle/m (0.5 and 0.4 m/cycle) corresponding to the 23 and 19 kyr precession component. The presence of both the 19 and 23 kyr precession component is a strong indication for orbital forcing of the ODP Site 959 Fe record (Herbert et al. 1995; Westerhold et al. 2007).

Following the metronome approach of Herbert et al. (1995), we first built a cyclostratigraphy by extracting and counting short eccentricity cycles in the Fe data using a Gaussian band-pass filter (Supplementary Fig. 2). Prior to tuning of the Fe record to orbital parameters, the phase relation between the terrigenous input in our study area and the orbital parameters has to be identified. Tiedemann et al. (1994) showed that maxima in the Pliocene dust flux record at 18°N correspond to maxima in precession (minima in northern hemisphere summer insolation). In addition, dust flux is clearly modulated by eccentricity reaching a maximum in short (100 kyr) eccentricity maxima and a minimum in the long (405 kyr) eccentricity cycle minima (see Tiedemann et al. 1994; Fig. 6 therein). Similarly, the Fe content in Miocene to early Pliocene records offshore of southern Africa increased during wet intervals occurring at eccentricity and obliquity maxima (Vidal et al. 2002; Westerhold et al. 2005).

We compared Site 959 Fe intensity data and Site 959 *C. wuellestorfi* oxygen isotope record (Norris 1998). Although both records differ in length and resolution, high Fe intensities correspond to high benthic oxygen isotope values suggesting Fe peaks correlate to northern hemisphere insolation maxima (precession minima). Based on the findings of Tiedemann et al. (1994) and assuming a constant phase relationship, we first tuned long eccentricity related Fe intensity minima to 405-kyr eccentricity minima using La2004 (Laskar et al. 2004) (Supplementary Fig. 3). For fine-tuning, we used the sum of normalized Eccentricity, Tilt and Precession (E + T − P) based on the La2004 solution (Laskar et al. 2004) as a target curve applying a minimum number of tie-points (Table 1). The resulted tuned Fe record and the calculated sedimentation rate varying between 1.47 and 2.96 cm/kyr are presented in Fig. 5.

Table 1 Age model for Late Miocene-Early Pleistocene Site 959 after tuning Fe intensity data to the ETP curve

Depth (rmcd)	Age (Ma)
21.90	1.862
22.03	1.871
25.98	2.139
27.74	2.258
38.47	2.948
42.60	3.154
45.77	3.326
47.52	3.440
55.85	3.842
61.90	4.076
76.55	4.715
80.05	4.851
83.38	5.069
87.07	5.216
89.70	5.379
91.40	5.446
96.73	5.652
101.04	5.805
103.57	5.899
109.75	6.107
112.70	6.206

To verify the accuracy of our age model, we compared the benthic oxygen isotope record at ODP Site 959 (Norris 1998) and several other tuned oxygen isotope records of ODP Sites 846, 926, 982 (Shackleton et al. 1995; Shackleton and Crowhurst 1997; Hodell et al. 2001) and the benthic oxygen isotope stack LR04 (Lisiecki and Raymo 2005). The heavy Marine Isotope Stages CN6 (4.41 Ma), Si6 (4.89 Ma) and TG20–22 (5.76–5.79 Ma) are well recognized and aligned as are the light Isotope Stages T5–T7 (5.09–5.13 Ma) (terminology after Shackleton et al. 1995). The major stepwise deglaciation from TG14 to TG9 between 5.6 and 5.5 Ma is also recognized. However, resulting ages of Stages TG9 through TG14 are about 50 ka

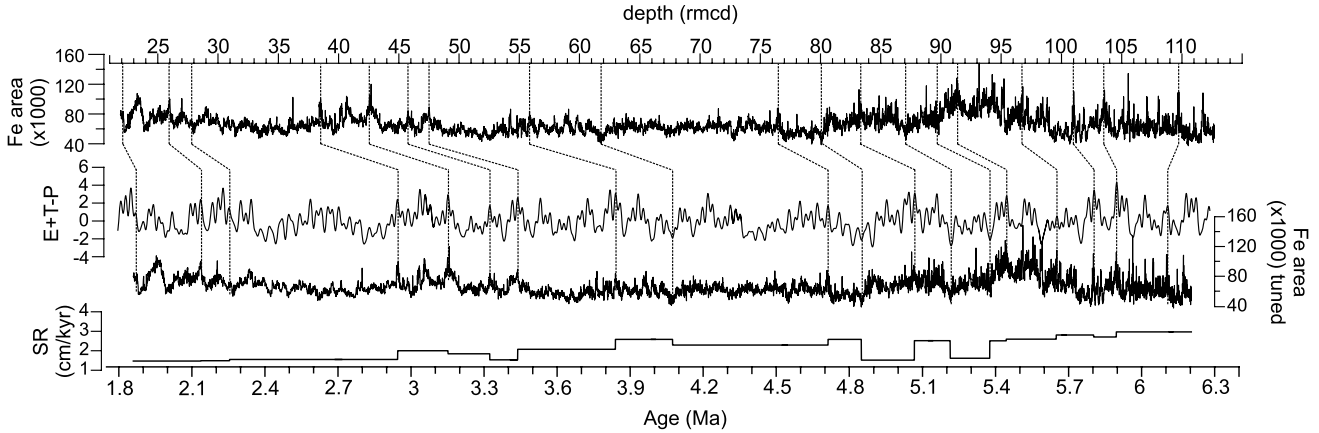

Fig. 5 Fine orbital tuning of Fe intensity data (Fe area). From *top* to *bottom* Site 959 Fe intensities on metre composite depth (rmcd); ETP curve calculated using La2004 solution (Laskar et al. 2004) and applied tie-points; tuned Fe intensity data on age and resulted sedimentation rate (SR). AnalySeries software (Paillard et al. 1996) has been used for tuning process

older at Site 959 than at Sites 926 and 982 (Supplementary Fig. 4).

Sedimentation at ODP Site 959

Interpretation of the elemental ratios in the sediment

Variations of Ti/Al, Ti/Ca, Al/Si ratios in the sediments of ODP Site 959 are discussed below as indicators of environmental change. Calcium in the Atlantic surface sediments derives mostly from marine biogenic carbonates (Arz et al. 1999; Govin et al. 2012) while Fe, Ti, Al and Si have mostly terrestrial sources.

Silicon is the most abundant element in mineral dust where it is the main constituent of coarse quartz grains (Scheuvens et al. 2013) and Al is linked to fine river clays (Collins et al. 2013). We, therefore, relate the Al/Si ratios to grainsize. Previous grain size analyses indicated that tropical rivers discharge mostly mud and very fine silt (<6 μm), while in the aeolian dust most grains range from fine to coarse silt (Sarnthein and Koopmann 1980; Weltje and Prins 2003). Dust coming from Sahelian and Saharan regions consists mainly of quartz grains and is enriched in silicon (Scheuvens et al. 2013; Collins et al. 2013). The grain size of dust collected off Ivory Coast/Ghana ranges from fine to coarse silt (10–40 μm) and becomes finer eastwards (Stuut et al. 2005).

Possible sources of Fe are iron oxides and hydroxides (hematite and goethite) that are a component of the distal aeolian dust (Balsam et al. 1995). Titanium is associated with coarse grain size minerals and due to its high content in aerosol samples, Ti has been proposed as an indicator for Saharan dust (Nicolás et al. 2008). Records of both Fe and Ti show similar patterns at Site 959, albeit Ti area values are substantially smaller. An excellent linear correlation has been found between ln(Ti/Ca) and dust percentages determined from the carbonate free siliciclastic content of sediments of ODP Site 659 (Tiedemann et al. 1994; Vallé et al. 2014). Thus, we interpret the Ti/Ca ratio in the sediment as an indication of the dust supply (Arz et al. 1999) and the Ti/Al ratio as a proxy of aeolian versus fluvial input (Govin et al. 2012; Zabel et al. 2001).

Sedimentation during the Messinian Salinity Crisis (MSC)

The ODP Site 959 sequence is one of the few sites in the East Atlantic that preserve a continuous record over the Messinian Salinity Crisis (Wagner 2002), which lasted from 5.97 to 5.33 Ma (Krijgsman et al. 1999; Manzi et al. 2013). Severe carbonate dissolution occurred in the oceans during the MSC (Wagner 2002) resulting in lower calcium intensities between 5.6 and 5.4 Ma (in Fig. 2 between 80 and 85 mbsf) and a moderate to poor preservation of foraminifera during Stages TG8 through TG14 (Norris 1998). Note that our age model results in 50 ka older ages for this interval than the established Mediterranean time scale (Roveri et al. 2008). The relatively high Ti/Ca ratios in sediments of Site 959 during the later stage of the MSC probably are the result of an overprint of poor carbonate preservation (Fig. 6).

Despite inferred carbonate dissolution, the calculated sedimentation rates are higher than in the rest of the record (~3 cm/kyr) and the terrestrial elements (Fe, Al, Ti) of Site 959 show elevated values between 5.6 and 5.4 Ma (Figs. 2, 5) corresponding with the last stage of the MCS, in which the Mediterranean Basin was mostly isolated from the Atlantic Ocean (5.55–5.33 Ma; CIESM 2008; Roveri et al. 2014). A comparable sedimentary pattern of increased

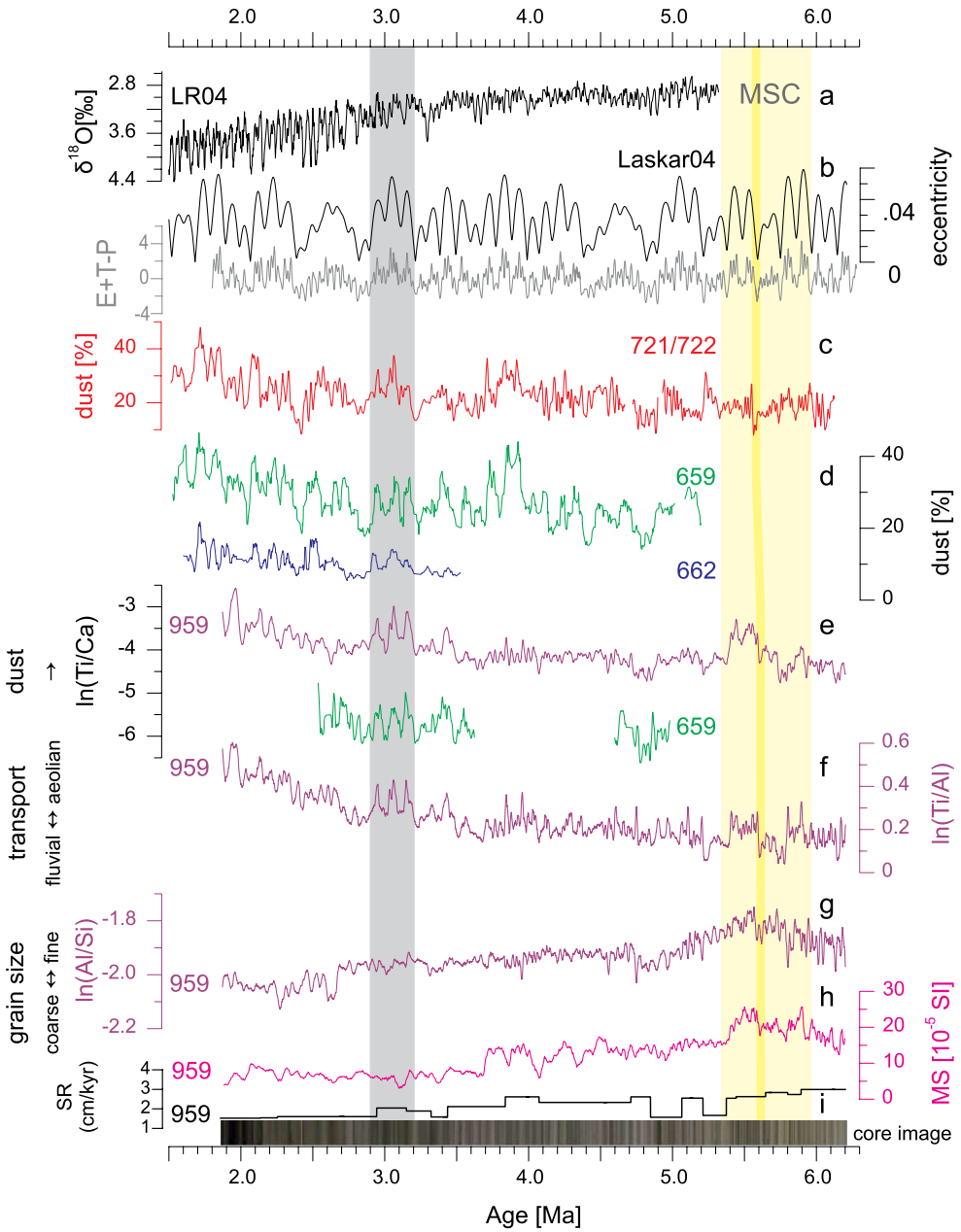

Fig. 6 **a** LR04 global oxygen isotope stratigraphy (Lisiecki and Raymo 2005). **b** Eccentricity (*black*) and E + T − P (*grey*) after Laskar et al. (2004). **c** Estimate of dust over the Arabian Sea after magnetic susceptibility from ODP Sites 721/722 (deMenocal 1995), in *red* 11 pt moving average. **d** Dust over the tropical East Atlantic from Site 659 (*green*) after Tiedemann et al. (1994) and Site 662 (*blue*) after Ruddiman and Janecek (1989), 11 pt moving averages; age model of Site 662 after Lisiecki and Raymo (2005) and (Herbert et al. 2010). **e** Ti/Ca ratios after XRF scanning of Site 959 (*violet*, this study) and Site 659 (*green*, Vallé et al. 2014), 31 pt moving averages. **f**, **g** Ti/Al (**f**) and Al/Si (**g**) ratios of Site 959 (*violet*, this study), 31 pt moving average. **h** Magnetic susceptibility of Site 959 (Mascle et al. 1996), in *magenta* 11 pt moving average, age model of this study. **i** Site 959 sedimentation rates (SR) and composite core image. *Light yellow shading* denotes the Messinian Salinity Crisis (MSC, 5.97–5.33 Ma, Manzi et al. 2013) and dark yellow shading the period 5.60–5.55 Ma (when the connection between Atlantic and Mediterranean was severed). For the period from 5.7 to 5.4 Ma, our age model deviates by 0.05 Ma from the established Mediterranean chronology (supplementary information). *Grey shading* denotes a period with high eccentricity overlapping the mid-Pliocene Warm Period (2.9–3.2 Ma). Localities of ODP Sites 659, 662 and 959 are given in Fig. 1

terrestrial input during the later stage of the MSC has been recorded at ODP Site 1085 in the South Atlantic by Vidal et al. (2002).

Sedimentary Al/Si ratios indicating smaller grain sizes and more fluvial mud increased between 6 and 5 Ma, fluctuated around intermediate levels between 5 and 2.7 Ma

and dropped to lower values afterwards, which suggests that fluvial sedimentation decreased after the MSC but did not cease before the late Pliocene. Increased fluvial input is also indicated by the higher magnetic susceptibility at Site 959 during the MSC (Mascle et al. 1996). A drop in sea level might have enhanced the river supply to the site (Wagner 2002), which today receives only little fluvial material from the Ghanaian slope explaining the low Pleistocene sedimentation rates (Giresse et al. 1998).

Tropical marine areas close to the continental margin are very sensitive to changes in continental freshwater run-off, especially during wetter intervals (Beckmann et al. 2005). Schneck et al. (2010) modelled a strong increase in precipitation in southern West Africa in sensitivity experiments with low sea level (−1500 m) in the Mediterranean Basin and a desiccated basin covered with grassy vegetation. Using the Community Atmosphere Model, Murphy et al. (2009) found increased precipitation in southern West Africa only in the low sea experiment, when sea level also had been lowered by 1500 m. From the model studies, a wetter climate and increased run-off in southern West Africa would be expected during the last stage of the MSC (5.55–5.33 Ma) when the connection between Mediterranean and Atlantic was restricted or severed. However, enhanced continental run-off along the West African coastline as indicated at Site 959 by lower Ti/Al ratios (more fluvial input) and higher Al/Si ratios (more fine fluvial mud) took place mainly before (5.8–5.6 Ma) and after (5.4–5.2 Ma) but not during the final stage of the MSC. On the other hand, indications of increased fluvial sedimentation correlate well with pronounced minima in the eccentricity curve (Fig. 6). Thus, it seems that the influence of the MSC on the climate in southern West Africa was limited and, more likely, stronger monsoon rains increased river discharge.

Long-term sedimentation changes after the MSC

After the MSC, records of Ti/Ca and Ti/Al have similar patterns (Fig. 6). We interpret them as a proxy for dust input and a proxy for aeolian versus fluvial supply, respectively. From 3.5 Ma, the higher Ti/Ca and Ti/Al ratios indicate a gradual increase of windblown dust reaching Site 959 and a reduction in fluvial supply. A long-term decrease of fluvial material—relative to other terrigenous material—from the late Miocene to the early Pleistocene is also indicated by the magnetic susceptibility record (Mascle et al. 1996) and by the increase in grain size particles as indicated by the Al/Si ratios (Fig. 6). A coarse resolution record of smear slides (Mascle et al. 1996) indicates that in the windblown dust the sand fraction increased and the clay fraction decreased from 4.9 Ma on. Gradual reduction of river discharge is seemingly contradictory to the increase in moist forest and swamps between 6.5 and 3 Ma as recorded by pollen from offshore Niger Delta boreholes (Morley 2000). However, decrease of fluvial input during the earliest Pliocene might be related to the initiation of the Guinean Current. Before the early Pliocene the West African coastline was closer to the equator, approximate at 2.5°N (Norris 1998) impeding the entrance of the Guinean current into the Guinea Gulf and implying a much northern position of the ITCZ relative to the coast (Norris 1998; Wagner 2002). This could have facilitated river supply to the marine site. From the reconstruction of the thermocline using stable oxygen isotope gradients of planktonic foraminifera, the initiation of the Guinea Current has been dated at ca. 4.9 Ma (Norris 1998; Billups et al. 1999; Wagner 2002), which amounts to ca. 5.2 Ma in the present age model.

Since 3.5 Ma, a stepwise or gradual southward shift in the average southernmost position of the ITCZ during winter would have allowed the NE trade winds to reach the Gulf of Guinea. After 2.9 Ma, the dust records of ODP Sites 659 and 721/722 show an increasing trend superimposed on the eccentricity fluctuations (Tiedemann et al. 1994; deMenocal 1995). The Ti/Ca ratios of ODP Site 959 increase since 2.75 Ma indicating more dust and the Al/Si ratios drop to a lower level at 2.7 Ma indicating coarser grain sizes. We link both changes to the enhanced dust export out of West Africa and the intensification of the northern hemisphere glaciations (e.g. De Schepper et al. 2014). From the pollen record of ODP Site 659, it has been concluded that NE trade winds strongly enhanced during short periods around 2.7 and 2.6 Ma and after 2.53 Ma (Leroy and Dupont 1994; Vallé et al. 2014) corresponding with increased aeolian input and cold sea surface temperatures at IODP Site U1313 in the North Atlantic (Naafs et al. 2012).

Eccentricity forcing of the climate in northern Africa

The sedimentary record indicates the influence of eccentricity cycles on the climate of northern Africa. Spectral analysis of ODP Site 959 elemental ratios indicates cyclic fluctuations in the eccentricity bands (100 and 405 kyr; Fig. 7). We calculated a wavelet analysis (Torrence and Compo 1998) and REDFIT spectra (Schulz and Mudelsee 2002). Specifically, the 405-kyr long eccentricity cycle is present in the Ti/Ca and Ti/Al dust records and the 100-kyr cycle becomes significant after 3.7 Ma. This is probably not an artefact of tuning, which was done on the Fe counts using the short eccentricity cycle and the ETP curve. Effects of changing sedimentation rates should be cancelled out by the use of ratios instead of concentrations. Influence of eccentricity on carbonate and organic carbon records of ODP Site 959 was already postulated by Wagner (2002) using the original biostratigraphic age model. High

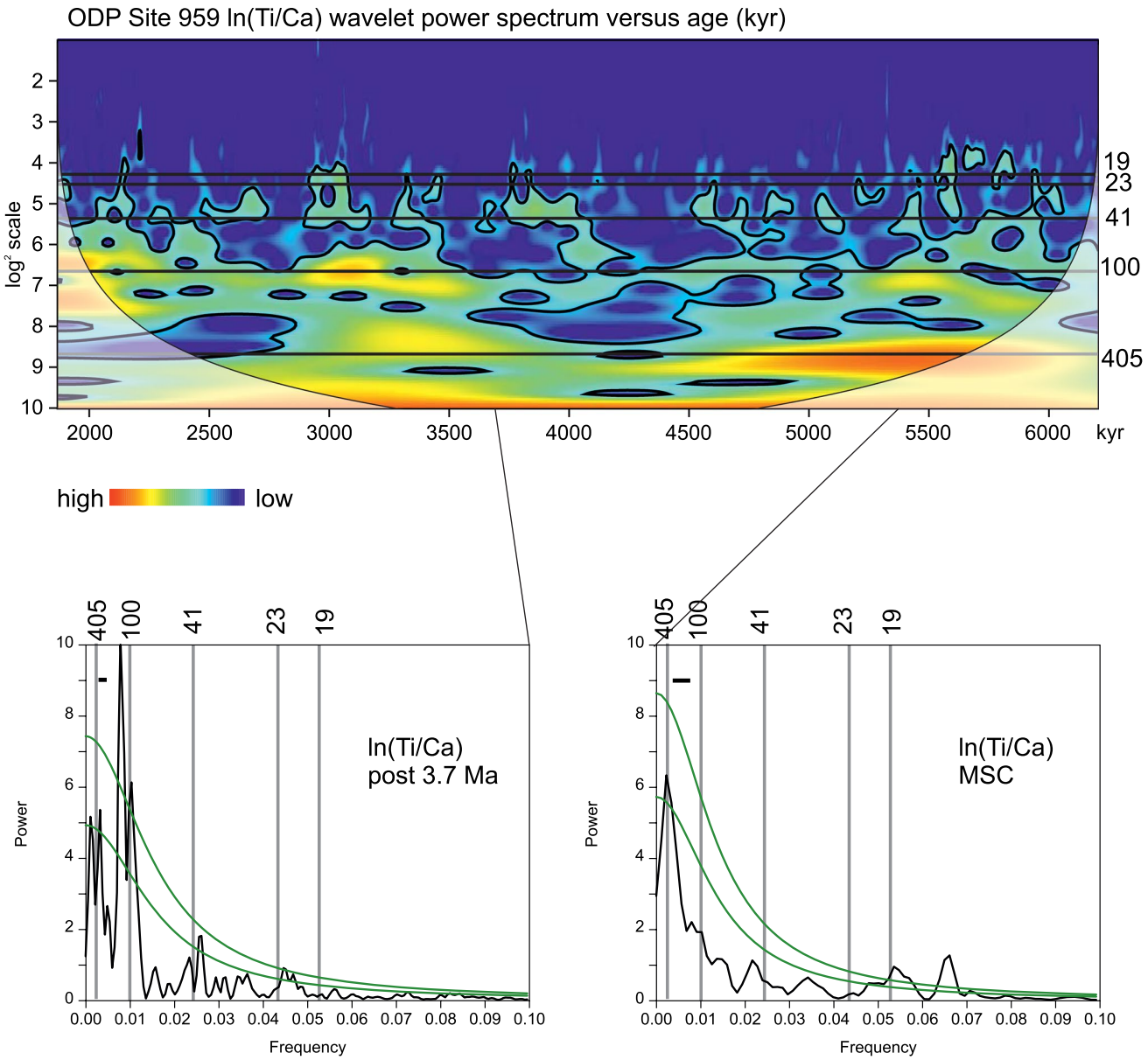

Fig. 7 *Top* Wavelet (Morlet) power spectrum of ln(Ti/Ca) on age in kyr. The data were detrended and linearly resampled at 1 kyr intervals. The contours are normalized linear variances with *blue* representing low spectral power and *red* representing high spectral power. The *black contour lines* enclose regions with more than 95 % confidence based on white noise. *Shaded areas* on either end indicate the cone of influence where padding with zeros influences the results. Orbital periodicities are indicated. *Bottom* Redfit power spectra (Schulz and Mudelsee 2002) of ln(Ti/Ca) data on age (not resampled) for two intervals, after 3.7 Ma (*left*) and before 5.4 Ma (*right*) using Welch overlapped segment averaging (three segments and ×2 oversampling). Confidence levels (80 %, 95 %) are calculated using a *red* noise model. *Grey bars* denote orbital periodicities. Wavelet spectrum and Redfit spectra were calculated with PAST software (Hammer et al. 2001)

precession variability is tied to eccentricity maxima. Marzocchi et al. (2015) modelled a full precession cycle and its consequences for the African monsoon system during the Miocene concluding that the African monsoon was already highly sensitive to orbital fluctuations during the Miocene. Indeed, Beckmann et al. (2005) documented precession and eccentricity cycles in the freshwater discharge along the Ivorian Margin for the Cretaceous.

Dust probably did not regularly reach the Gulf of Guinea prior to 3.5 Ma. While the dust records of Site 659 (18°N East Atlantic) and Site 721/722 (17°N Arabian Sea) indicate dust outbreaks during periods with strong eccentricity, especially shortly after 4 Ma, Site 959 from the Ivory Basin reveals no such marked fluctuations (Fig. 6). In the time domain, the Ti/Ca ratios of ODP Site 959 exhibit three noticeable dust maxima between 3.2 and 2.9 Ma

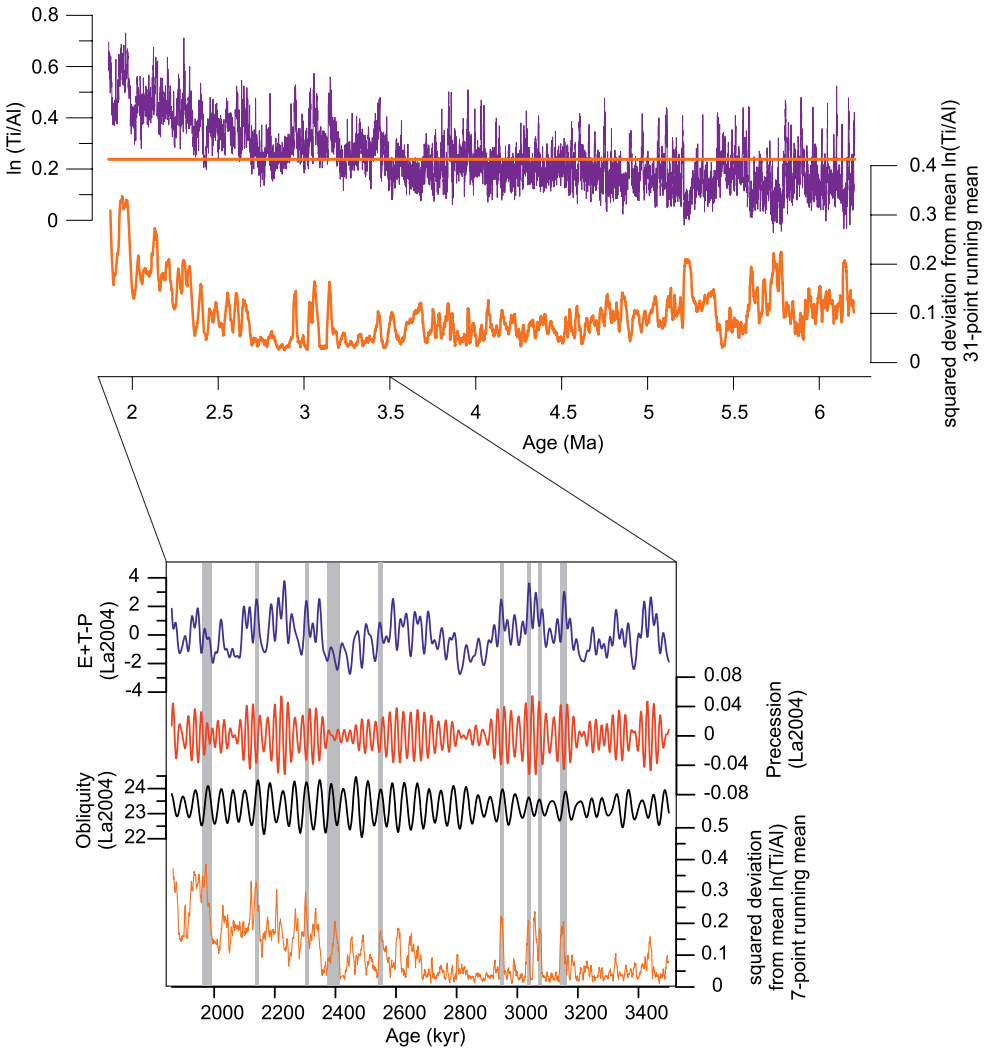

Fig. 8 From *top* to *bottom* ln(Ti/Al) ratio, squared deviation from the mean value over the studied interval (31-point running mean), E + T − P curve, precession, obliquity, and squared deviation from the mean (7-point running mean). Insolation curves after (Laskar et al. 2004). Stronger seasonality is suggested by the squared deviation from the mean value of the ln(Ti/Al) occurring between 5.8 and 5.5 Ma, between 5.3 and 5.2 Ma and increased after 3.2 Ma

corresponding with eccentricity maxima. These maxima have been found in other dust records of northern Africa, at ODP Sites 659 and 662 retrieved from the East Atlantic (Ruddiman and Janecek 1989; Tiedemann et al. 1994) as well as at ODP Site 721/722 from the Arabian Sea of (deMenocal 1995). Those records have been plotted in Fig. 6 on their original time scales, except for ODP Site 662 in the equatorial East Atlantic, which age model has been tuned by Lisiecki and Raymo (2005) and improved by Herbert et al. (2010). Correspondence of the dust records over such a large area suggests continent-wide aridity—or at least large climate variability with enhanced winds and expansion of desert-like regions to produce the dust. The dusty periods in northern Africa between 3.2 and 2.9 Ma have no counterpart in North America where substantial dust production did not start before 2.72 Ma (Lang et al. 2014). The African dusty periods indicate large climate variability and probably strong seasonal variations during the mid-Piacenzian Warm Period (3.3–3.0 Ma; Prescott et al. 2014). In contrast, minimal dust was found in all three records (ODP Sites 659, 721/722, 959) between 4.9 and 4.7 Ma. This minimum corresponds to one of the very long eccentricity minima in eccentricity during the early Pliocene implying smaller amplitudes of precession cycles (Fig. 6).

If strong monsoon variability implies strong seasonality, we might interpret the Ti/Al ratios in terms of seasonality (Beckmann et al. 2005). Stronger seasonality is suggested by the deviation from the mean value of the Ti/Al ratios and would have occurred between 5.8 and 5.5 Ma, between 5.3

and 5.2 Ma and increased after 3.2 Ma (Fig. 8). Between 3.4 and 1.82 Ma, those periods of enhanced seasonality occurred during obliquity maxima and precession minima. This would fit modelling by Tuenter et al. (2005) indicating that both precession and obliquity intensify precipitation seasonality in northern Africa.

Conclusions

XRF scanning of cores from three drilled holes of ODP Site 959 off tropical West Africa (Ivory Basin) provided high-resolution major element intensities for the Late Miocene to Early Pleistocene. We used the Fe intensity record to obtain a new composite depth scale and an orbital-tuned age model from 6.20 to 1.82 Ma.

Variations of elemental ratios record a long-term decrease of fluvial supply to ODP Site 959 from the Late Miocene to the Early Pleistocene probably related to the beginning of the Guinean Current and a southward shift of the Intertropical Convergence Zone. Time series analysis underlines the importance of eccentricity and precession (modulated by eccentricity) on the sedimentary cycles of Site 959.

During the earlier stages (but not the final ones) of the Mediterranean Salinity Crisis, the Ti/Al ratios of ODP Site 959 sediments suggest increased precipitation and river run-off along the southern West African coast corresponding with eccentricity minima. The record of siliciclastic supply at Site 959 suggests that winter dust was regularly reaching the Gulf of Guinea after 3.5 Ma. The Ti/Al record suggests increased seasonality during obliquity maxima and precession minima from 3.4 Ma on. Comparing several dust records indicate increased continental aridity and/or enhanced climate variability in northern Africa during eccentricity maxima between 3.2 and 2.9 Ma. From 2.9 Ma on, the trend in ODP Site 959 elemental ratios indicates increasing impact of northern hemisphere glaciations on the climate of West Africa.

Acknowledgments The study was financially supported by the Deutsche Forschungsgemeinschaft (DFG), Grant DU221/5. FV thanks GLOMAR (Bremen International Graduate School for Marine Sciences). We thank Ocean Drilling Program for providing the samples. Alexus Wülbers, Dr. Walter Hale, Vera Lukies, and Dr. Ursula Röhl are gratefully acknowledged for helping with core handling and XRF scanning. Data are stored at Pangaea.de. The paper gained a lot from the constructive and helpful comments of Ian Bailey and an anonymous reviewer.

Authors' contribution F. V. conducted the XRF measurements, developed the composite depth and astronomical age model, interpreted the results, and drafted the article; T. W. developed the composite depth and astronomical age model, interpreted the results, drafted and revised the article; L. M. D. interpreted the results, drafted and revised the article.

References

Arz H, Pätzold J, Wefer G (1999) The deglacial history of the western tropical Atlantic as inferred from high resolution stable isotope records off northern Brazil. Earth Planet Sci Lett 167:105–117

Bailey I, Hole GM, Foster GL, Wilson PA, Storey CD, Trueman CN, Raymo ME (2013) An alternative suggestion for the Pliocene onset of major northern hemisphere glaciation based on the geochemical provenance of North Atlantic Ocean ice-rafted debris. Quat Sci Rev 75:181–194

Balsam WL, Otto-Bliesner BL, Deaton BC (1995) Modern and last glacial maximum eolian sedimentation patterns in the Atlantic Ocean interpreted from sediment iron oxide content. Paleoceanography 10:493–507

Beckmann B, Flögel S, Hofmann P, Schulz M, Wagner T (2005) Orbital forcing of Cretaceous river discharge in tropical Africa and ocean response. Nature 437:241–244

Billups K, Ravelo AC, Zachos JC, Norris RD (1999) Link between oceanic heat transport, thermohaline circulation, and the Intertropical Convergence Zone in the early Pliocene Atlantic. Geology 27:319–322

Boko M, Niang I, Nyong A, Vogel C, Githeko A, Medany M, Osman-Elasha B, Tabo R, Yanda P (2007) Climate change 2007: impacts, adaptation and vulnerability. In: Parry ML, Canziani OF, Palutikov JP, Van der Linden PJ, Hanson CE (eds) Contribution of working group II to the fourth assessment report of the intergovernmental panel on climate change. Cambridge University Press, Cambridge, pp 433–467

Brierley CM, Fedorov AV (2010) Relative importance of meridional and zonal sea surface temperature gradients for the onset of the ice ages and Pliocene–Pleistocene climate evolution. Paleoceanography 25:PA2214. doi:10.1029/2009PA001809

Brierley CM, Fedorov AV, Liu Z, Herbert TD, Lawrence KT, LaRieviere JP (2009) Greatly expanded tropical warm pool and weakened hadley circulation in the early Pliocene. Science 323:714–718

CIESM (2008) The Messinian Salinity Crisis from mega-deposits to microbiology. In: Briand F (ed) A consensus report, in 33 CIESM workshop monographs, 33. CIESM, 16, bd de Suisse, MC-98000, Monaco, pp 1–168

Collins JA, Govin A, Mulitza S, Heslop D, Zabel M, Hartmann J, Röhl U, Wefer G (2013) Abrupt shifts of the Sahara–Sahel boundary during Heinrich stadials. Clim Past 9:1181–1191. doi:10.5194/cp-9-1181-2013

De Schepper S, Gibbard PL, Salzmann U, Ehlers J (2014) A global synthesis of the marine and terrestrial evidence for glaciation during the Pliocene Epoch. Earth Sci Rev 135:83–102

deMenocal P (1995) Plio-Pleistocene African climate. Science 270:53–59

deMenocal P (2011) Climate and human evolution. Science 331:540–542

Evans HF, Westerhold T, Channell JET (2004) ODP site 1092: revised composite depth section has implications for Upper Miocene "cryptochrons". Geophys J Int 156:195–199

Fedorov AV, Brierley CM, Lawrence KT, Liu Z, Dekens PS, Ravelo AC (2013) Patterns and mechanisms of early Pliocene warmth. Nature 496:43–49

Ghil M, Allen MR, Dettinger MD, Ide K, Kandrashov D, Mann ME, Robertson AW, Sanders A, Tian Y, Varadi F, Yiov P (2002) Advanced spectral methods for climatic timeseries. Rev Geophys 40:1003. doi:10.1029/2001RG000092

Giresse P, Gadel F, Serve L, Barusseau JP (1998) Indicators of climate and sediment-source variations at Site 959: implications for the reconstruction of the paleoenvironments in the Gulf of Guinea through Pleistocene times. In: Mascle J, Lohmann GP,

Moullade M (eds) Proceedings of the Ocean Drilling Program, Scientific Results, 159. Ocean Drilling Program, College Station, pp 585–603

Govin A, Holzwarth U, Heslop D, Ford-Keeling L, Zabel M, Mulitza S, Collins JA, Chiessi CM (2012) Distribution of major elements in Atlantic surface sediments (36°N–49°S): imprint of terrigenous input and continental weathering. Geochem Geophys Geosyst 13:Q01013. doi:10.1029/2011GC003785

Hammer Ø, Harper DAT, Ryan PD (2001) PAST: Paleontological statistics software package for education and data analysis. Palaeontol Electr 4:1–9

Haywood AM, Dowsett HJ, Dolan AM (2016) Integrating geological archives and climate models for the mid-Pliocene warm period. Nat Commun 7:10646. doi:10.1038/ncomms10646

Hennissen JAI, Head MJ, De Schepper S, Goeneveld J (2015) Increased seasonality during the intensification of northern hemisphere glaciation at the Pliocene–Pleistocene boundary ~2.6 Ma. Quat Sci Rev 129:321–332

Herbert T, Premoli Silva I, Erba E, Fischer AG (1995) Orbital chronology of cretaceous-paleocene marine sediments. Geochronology time scales and global stratigraphic correlation, SEPM special publication no. 54

Herbert TD, Cleaveland Peterson L, Lawrence KT, Liu Z (2010) Tropical ocean temperatures over the past 3.5 million years. Science 328:1530–1534

Hodell DA, Curtis JH, Sierro JF, Raymo ME (2001) Correlation of the late Miocene to early Pliocene sequences between the Mediterranean and North Atlantic. Paleoceanography 16:164–178

Ivanovic RF, Valdes PJ, Flecker R, Gutjahr M (2014) Modelling global-scale climate impacts of the late Miocene Messinian Salinity Crisis. Clim Past 10:607–622

Kalu AE (1979) The African dust plume: its characteristics and propagation across West Africa in Winter. In: Morales C (ed) Saharan dust: mobilization, transport, deposition. Wiley, New York, pp 95–118

Kouwenhoven TJ, Van der Zwaan GJ (2006) A reconstruction of late Miocene Mediterranean circulation patterns using benthic foraminifera. Palaeogeogr Palaeoclimatol Palaeoecol 238:373–385

Krijgsman W, Hilgen FJ, Raffi I, Sierro FJ, Wilson DS (1999) Chronology, causes and progression of the Messinian Salinity Crisis. Nature 400:652–655

Kutzbach JE, Liu Z (1997) Response of the African monsoon to orbital forcing and ocean feedbacks in the middle Holocene. Science 278:440–443

Lang DC, Bailey I, Wilson P, Beer CJ, Bolton CT, Friedrich O, Newsam C, Spencer MR, Gutjahr M, Foster GL, Cooper MJ, Milton JA (2014) The transition on North America from the warm humid Pliocene to the glaciated Quaternary traced by eolian dust deposition at a benchmark North Atlantic Ocean drill site. Quat Sci Rev 93:125–141

Larrasoaña JC, Roberts AP, Rohling EJ (2013) Dynamics of green Sahara periods and their role in hominin evolution. PLoS One 8:e76514. doi:10.1371/journal.pone.0076514

Laskar J, Robutel P, Joutel F, Gastineau M, Correia ACM, Levrard B (2004) A long-term numerical solution for the insolation quantities of the Earth. Astron Astrophys 285:261–285

Lawrence KT, Sosdian S, White HE, Rosenthal Y (2010) North Atlantic climate evolution through the Plio-Pleistocene climate transitions. Earth Planet Sci Lett 300:329–342

Leroy SAG, Dupont LM (1994) Development of vegetation and continental aridity in northwestern Africa during the Late Pliocene: the pollen record of ODP Site 658. Palaeogeogr Palaeoclimatol Palaeoecol 109:295–316

Lisiecki LE, Raymo ME (2005) A Pliocene–Pleistocene stack of 57 globally distributed benthic $\delta^{18}O$ records. Paleoceanography 20:PA1003. doi:10.1029/2004PA001071

Mann ME, Lees JM (1996) Robust estimation of background noise and signal detection in climatic time series. Clim Change 33:409–445. doi:10.1007/BF00142586

Manzi V, Gennari R, Hilgen F, Krijgsman W, Lugli S, Roveri M, Sierro FJ (2013) Age refinement of the Messinian Salinity Crisis onset in the Mediterranean. Terra Nova 25:315–322

Martínez-Garcia A, Rosell-Mele A, Jaccard SL, Geibert W, Sigman DM, Haug GH (2011) Southern Ocean dust–climate coupling over the past four million year. Nature 476:312–316. doi:10.1038/nature10310

Marzocchi A, Lunt DJ, Flecker R, Bradshaw CD, Farnsworth A, Hilgen FJ (2015) Orbital control on late Miocene climate and the North African monsoon: insight from an ensemble of sub-precessional simulations. Clim Past Discuss 11:2181–2237

Mascle J, Lohmann GP, Clift PD et al (1996) Proceedings of the Ocean Drilling Program, Initial Reports, 159. Ocean Drilling Program, College Station

McGee D, Donohoe A, Marshall J, Ferreira D (2014) Changes in ITCZ location and cross-equatorial heat transport at the Last Glacial Maximum, Heinrich Stadial 1, and the mid-Holocene. Earth Planet Sci Lett 390:69–79

Morley RJ (2000) Origin and evolution of tropical rain forest. Wiley, London, p 378

Murphy LN, Kirk-Davidoff DB, Mahowald N, Otto-Bliesner BL (2009) A numerical study of the climate response to lowered Mediterranean Sea level during the Messinian Salinity Crisis. Palaeogeogr Palaeoclimatol Palaeoecol 279:41–59

Naafs DB, Hefter J, Acton G, Haug GH, Martínez-Garcia A, Pancost R, Stein R (2012) Strengthening of North American dust sources during the late Pliocene (2.7 Ma). Earth Planet Sci Lett 317–318:8–19

Nicholson SE (2009) A revised picture of the structure of the "monsoon" and land ITCZ over West Africa. Clim Dyn 32:1155–1171

Nicolás J, Chiari M, Crespo J, Garcia Orellana I, Lucarelli F, Nava S, Pastor C, Yubero E (2008) Quantification of Saharan and local dust impact in an arid Mediterranean area by the positive matrix factorization (PMF) technique. Atmos Environ 42:8872–8882

Norris RD (1998) Planktonic foraminifer biostratigraphy: eastern equatorial Atlantic. In: Mascle J, Lohmann GP, Moullade M (eds) Proceedings of the Ocean Drilling Program, Scientific Results, 159. Ocean Drilling Program, College Station, pp 539–555

Paillard D, Labeyrie L, Yiou P (1996) Macintosh program performs time-series analysis. EOS Trans AGU 77(39):379. doi:10.1029/96EO00259

Pérez-Asensio JN, Aguirre J, Schmiedl G, Civis J (2012) Impact of restriction of the Atlantic–Mediterranean gateway on the Mediterranean Outflow Water and eastern Atlantic circulation during the Messinian. Paleoceanography 27:PA3222. doi:10.1029/2012PA002309

Prescott CL, Haywood AM, Dolan AM, Hunter SJ, Popoe JO, Pickering SJ (2014) Assessing orbitally-forced interglacial climate variability during the mid-Pliocene Warm Period. Earth Planet Sci Lett 400:261–271

Prospero JM, Ginoux P, Torres O, Nicholson SE, Gill TE (2002) Environmental characterization of global sources of atmospheric soil dust identified with the Nimbus 7 total ozone mapping spectrometer (TOMS) absorbing aerosol product. Rev Geophys 40:1002. doi:10.1029/2000RG000095

Röhl U, Abrams LJ (2000) High resolution, downhole, and nondestructive core measurements from Site 999 and 1001 in the Caribbean sea: application to the Late Paleocene thermal maximum. In: Leckie RM, Sigurdsson H, Acton GD, Draper G (eds) Proceedings of the Ocean Drilling Program, Scientific Results, 165. Ocean Drilling Program, College Station, pp 191–203

Röhl U, Westerhold T, Bralower TJ, Zachos JC (2007) On the duration of the Paleocene–Eocene thermal maximum (PETM). Geochem Geophys Geosyst 8:Q12002. doi:10.1029/2007GC001784

Rohling EJ, Marino G, Grant KM (2015) Mediterranean climate and oceanography, and the periodic development of anoxic events (sapropels). Earth Sci Rev 143:62–97

Rossignol-Strick M, Nesteroff W, Olive P, Vergnaud-Grazzini C (1982) After the deluge: Mediterranean stagnation and sapropel formation. Nature 295:105–110

Roveri M, Lugli S, Manzi V, Schreiber CB (2008) The Messinian Sicilian stratigraphy revisited: new insights for the Messinian Salinity Crisis. Terra Nova 20:483–488

Roveri M, Flecker R, Krijgsman W, Lofi J, Lugli S, Manzi V, Sierro FJ, Bertini A, Camerlenghi A, de Lange G, Govers R, Hilgen FJ, Hübscher C, Meijer PTh, Stoica M (2014) The Messinian Salinity Crisis: past and future of a great challenge for marine sciences. Mar Geol 352:25–58

Ruddiman WF, Janecek T (1989) Pliocene–Pleistocene biogenic and terrigenous fluxes at equatorial Atlantic Sites 662, 663, and 664. In: Ruddiman W, Sarnthein M et al (eds) Proceedings Ocean Drilling Program, Scientific Results, 108. Ocean Drilling Program, College Station, pp 211–240

Ruddiman WF, Sarnthein M, Backman J, Baldauf JG, Curry W, Dupont LM, Janecek T, Pokras EM, Raymo ME, Stabell B, Stein R, Tiedemann R (1989) Late Miocene to Pleistocene evolution of climate in Africa and the low-latitude Atlantic: overview of Leg 108 results. In: Ruddiman WF, Sarnthein M et al (eds) Proceedings of the Ocean Drilling Program, Scientific Results, 108. Ocean Drilling Program, College Station, pp 463–484

Sarnthein M, Koopmann B (1980) Late Quaternary deep-sea record on Northwest African dust supply and wind circulation. Palaeoecol Afr 12:239–253

Sarnthein M, Tetzlaff G, Koopmann B, Wolter K, Pflaumann U (1981) Glacial and interglacial wind regimes over the eastern subtropical Atlantic and North-West Africa. Nature 293:193–196

Scheuvens D, Schütz L, Kandler K, Ebert M, Weinbruch S (2013) Bulk composition of northern African dust and its source sediments—a compilation. Earth Sci Rev 116:170–194

Schneck R, Micheels A, Mosbrugger V (2010) Climate modelling sensitivity experiments for the Messinian Salinity Crisis. Palaeogeogr Palaeoclimatol Palaeoecol 286:149–163

Schulz M, Mudelsee M (2002) REDFIT: estimating red-noise spectra directly from unevenly spaced paleoclimatic time series. Comput Geosci 28:421–426

Shackleton NJ, Crowhurst S (1997) Sediment fluxes based on an orbitally tuned time scale 5 Ma to 14 Ma, Site 926. In: Shackleton NJ, Curry WB, Richter C, Bralower T (eds) Proceedings of the Ocean Drilling Program, Scientific Results, 154. Ocean Drilling Program, College Station, pp 69–82

Shackleton NJ, Hall MA, Pate D (1995) Pliocene stable isotope stratigraphy of Site 846. In: Pisias NG, Mayer LA, Janecek TR, Palmer-Julson A, van Andel TH (eds) Proceedings of the Ocean Drilling Program, Scientific Results, 138. Ocean Drilling Program, College Station, pp 337–355

Stuut JB, Zabel M, Ratmeyer V, Helmke P, Schefuß E, Lavik G, Schneider R (2005) Provenance of present-day eolian dust collected off NW Africa. J Geophys Res 110:D04202. doi:10.1029/2004JD005161

Tiedemann R, Sarnthein M, Shackleton NJ (1994) Astronomic timescale for the Pliocene Atlantic $\delta^{18}O$ and dust flux records of Ocean Drilling Program site 659. Paleoceanography 9:619–638

Topper RPM, Meijer PTh (2013) A modeling perspective on spatial and temporal variations in Messinian evaporite deposits. Mar Geol 336:44–60

Torrence C, Compo GP (1998) A practical guide to wavelet analysis. Bull Am Meteorol Soc 79:61–78

Tuenter E, Weber SL, Hilgen FJ, Lourens LJ (2003) The response of the African summer monsoon to remote and local forcing due to precession and obliquity. Global Planet Change 36:219–235

Tuenter E, Weber SL, Hilgen FJ, Lourens LJ, Ganopolski A (2005) Simulation of climate phase lags in response to precession and obliquity forcing and the role of vegetation. Clim Dyn 24:279–295

Vallé F, Dupont LM, Leroy SAG, Schefuß E, Wefer G (2014) Pliocene environmental change in West Africa and the onset of strong NE Trade winds (ODP Sites 659 and 658). Palaeogeogr Palaeoclimatol Palaeoecol 414:403–414

Verstraete J-M (1992) The seasonal upwellings in the Gulf of Guinea. Prog Oceanogr 29:1–60

Vidal L, Bickert T, Wefer G, Röhl U (2002) Late Miocene stable isotope stratigraphy of SE Atlantic ODP Site 1085: relation to Messinian events. Mar Geol 180:71–85

Wagner T (1998) Pliocene–Pleistocene deposition of carbonate and organic carbonate at Site 959: paleoenvironmental implications for the eastern Equatorial Atlantic off Ivory Coast/Ghana. In: Mascle J, Lohmann GP, Moullade M (eds) Proceedings of the Ocean Drilling Program, Scientific Results, 159. Ocean Drilling Program, College Station, pp 557–574

Wagner T (2002) Late Cretaceous to early Quaternary organic sedimentation in the eastern Equatorial Atlantic. Palaeogeogr Palaeoclimatol Palaeoecol 179:113–147

Wara MW, Ravelo AC, Delaney ML (2005) Permanent El Nino-like conditions during the Pliocene Warm Period. Science 309:758–761

Weedon G (2003) Time-series analysis and cyclostratigraphy: examining stratigraphic records of environmental cycles. Cambridge University Press, Cambridge

Weltje GJ, Prins MA (2003) Muddled or mixed? Inferring palaeoclimate from size distributions of deep-sea clastics. Sediment Geol 162:39–62

Weltje GJ, Tjallingii R (2008) Calibration of XRF core scanners for quantitative geochemical logging of sediment cores: theory and application. Earth Planet Sci Lett 274:423–438

Westerhold T, Röhl U (2013) Orbital pacing of Eocene climate during the Middle Eocene Climate Optimum and the chron C19r event: missing link found in the tropical western Atlantic. Geochem Geophys Geosyst 14:4811–4825. doi:10.1002/ggge.20293

Westerhold T, Bickert T, Röhl U (2005) Middle to late Miocene oxygen isotope stratigraphy of ODP site 1085 (SE Atlantic): new constrains on Miocene climate variability and sea-level fluctuations. Palaeogeogr Palaeoclimatol Palaeoecol 217:205–222

Westerhold T, Röhl U, Laskar J, Raffi I, Bowles J, Lourens LJ, Zachos JC (2007) On the duration of magnetochrons C24r and C25n and the timing of early Eocene global warming events: Implications from the Ocean Drilling Program Leg 208 Walvis Ridge depth transect. Paleoceanography 22:PA2201. doi:10.1029/2006PA001322

Westerhold T, Röhl U, Wilkens R, Pälike H, Lyle M, Jones TD, Bown P, Moore T, Kamikuri S, Acton G, Ohneiser C, Yamamoto Y, Richter C, Fitch P, Scher H, Liebrand D, E. 320/321 Scientists (2012) Revised composite depth scales and integration of IODP Sites U1331-U1334 and ODP Sites 1218–1220. In: Pälike H, Lyle M, Nishi H, Raffi I, Gamage K, Klaus A, and the Expedition 320/321 Scientists, Proceedings IODP, 320/321, Tokyo (Integrated Ocean Drilling Program Management International, Inc.). doi:10.2204/iodp.proc.320321.201.2012

Zabel M, Schneider RR, Wagner T, Adegbie AT, de Vries U, Kolonic S (2001) Late Quaternary climate changes in central Africa as inferred from terrigenous input to the Niger Fan. Quat Res 56:207–217

Zhang Z, Ramstein G, Schuster M, Li C, Contoux C, Yan Q (2014) Aridification of the Sahara desert caused by Tethys Sea shrinkage during the Late Miocene. Nature 513:401–404